Joule, Volume *11*

Supplemental information

On-demand capacity extraction through thermo-electrochemical hysteresis in metastable Li-Cu alloy

Jun Ho Lee, Wenbo Zhang, Yusheng Ye, Sarah E. Holmes, Eder G. Lomeli, Sanzeeda Baig Shuchi, Sang Cheol Kim, Mun Sek Kim, Junyoung Lee, Il Rok Choi, Donglin Li, Huayue Ai, Philaphon Sayavong, Solomon T. Oyakhire, Malhar Kute, Thomas P. Devereaux, and Yi Cui

Note S1. Preparation of TEM samples

Our Li-Cu alloy particles were in micrometer-scale, and it was difficult to prepare samples for TEM, which should be in at least 100 nm scale. To overcome the dimension issue, we implemented another way of preparing Li-Cu alloy – melting separate foils of Li and Cu. Pristine Li and Cu foils with 62.2 at% of Li were melted in a stainless-steel tray on the hot plate at 400 °C. After complete mixing of Li and Cu, Cu coated lacey carbon TEM grid was dipped in to the solution to transfer Li-Cu. Li-Cu alloy transferred on to the TEM grid was further exposed to H_2O outside the Ar glove box to remove Li-rich phases. Supplementary Fig. 31 depicts that Cu-rich phase prepared in this method exhibited same XRD peaks with oven-annealing method we utilized for general studies. As-prepared TEM grids were transferred to TEM for further study.

Note S2. Parametric method for deciding solvus line of phase diagram.

To determine the boundaries of a two-phase region empirically, the lattice parameter of each phase is used. In a two-phase region, for example of A and B, the composition of A and B phases do not change and only their ratio changes with atomic concentration. Consequently, lattice parameters of A and B remain constant throughout the entire two-phase region. However, outside the region, they are subject to change because of solubility of each element to the other phase. Thus, the parametric method is to empirically find the atomic concentration whereby the lattice parameter starts to be a constant value. In this paper, the solvus line of Li-Cu binary phase diagram at 400 °C was of our interest. The two-phase region at 400 °C is composed of fcc-(Cu) and Li-rich phase, so the solubility limit of Li into fcc-(Cu) would be the location of solvus line for Li-Cu system. From this regard, we traced the change in Cu lattice parameter over a wide range of Li at% to estimate the at% of the solvus line with extrapolation. The intersect of two extrapolated lines, one from two-phase region and another from Cu to fcc-(Cu), is expected to be the solubility limit of Li into fcc-(Cu), and thus the chemical composition of fcc-(Cu), that is Cu_4Li. Bragg's law, $n\lambda = 2d \sin\theta$, is used to derive d_{hkl} of specific (hkl) plane from know and theta, whereas d_{hkl} can provide the lattice parameter d of FCC lattice from $d_{hkl} = \frac{d}{\sqrt{h^2+k^2+l^2}}$.

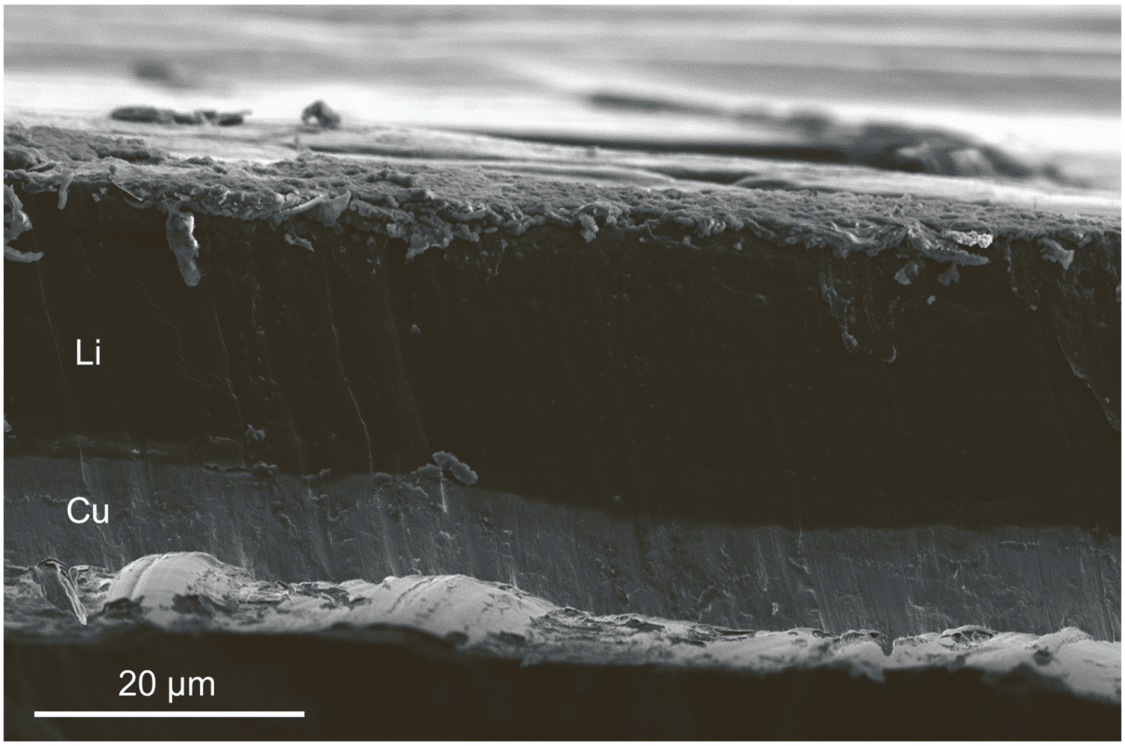

Figure S1 | Cross-sectional SEM image of pristine thin Li foil. 20 μm–thick Li deposited on 11 μm–thick Cu foil. (Tilt : -10°).

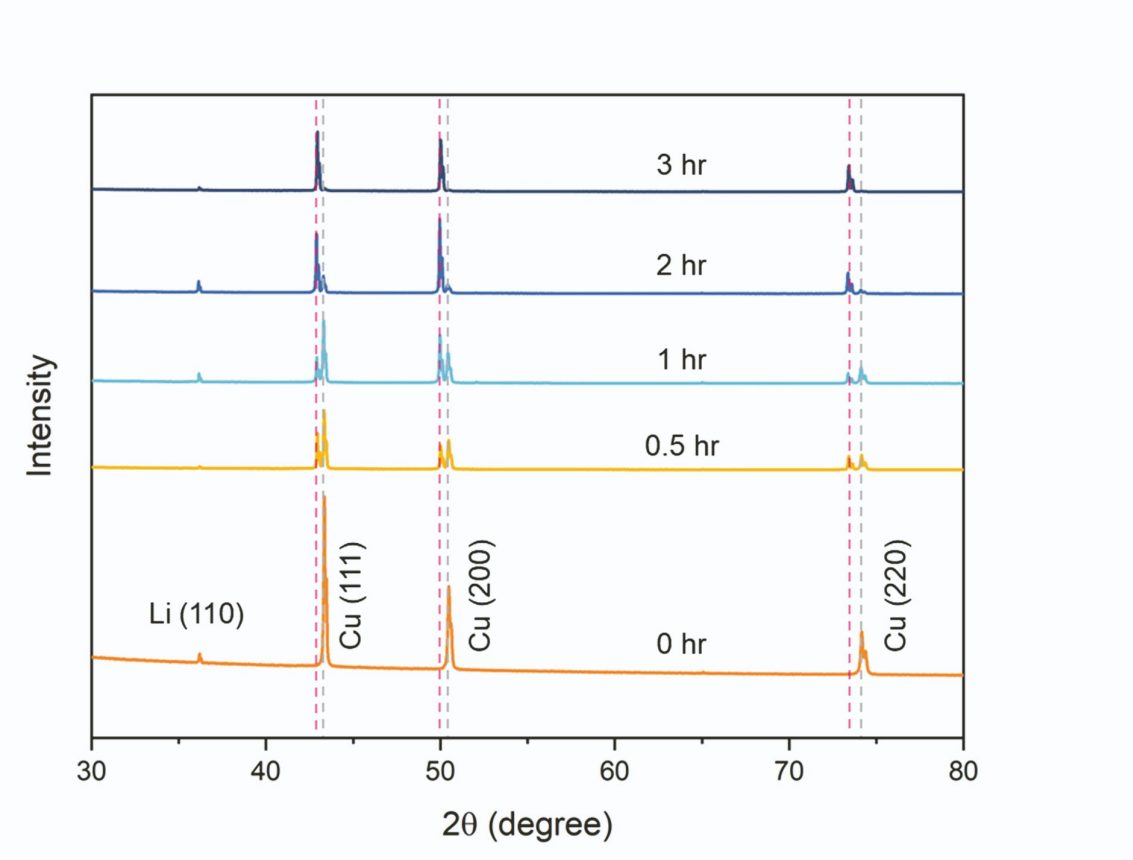

Figure S2 | XRD spectra of Li-Cu alloy on different annealing times. The annealing time was ranging from 0 hr (orange) to 0.5 hr (yellow), 1 hr (light blue), 2 hr (blue), and 3 hr (navy). Li(110), Cu (111), Cu (200), and Cu (220) peaks are marked with grey dashed lines. Peaks corresponding to new phase from Li-Cu alloy are marked with pink dashed line.

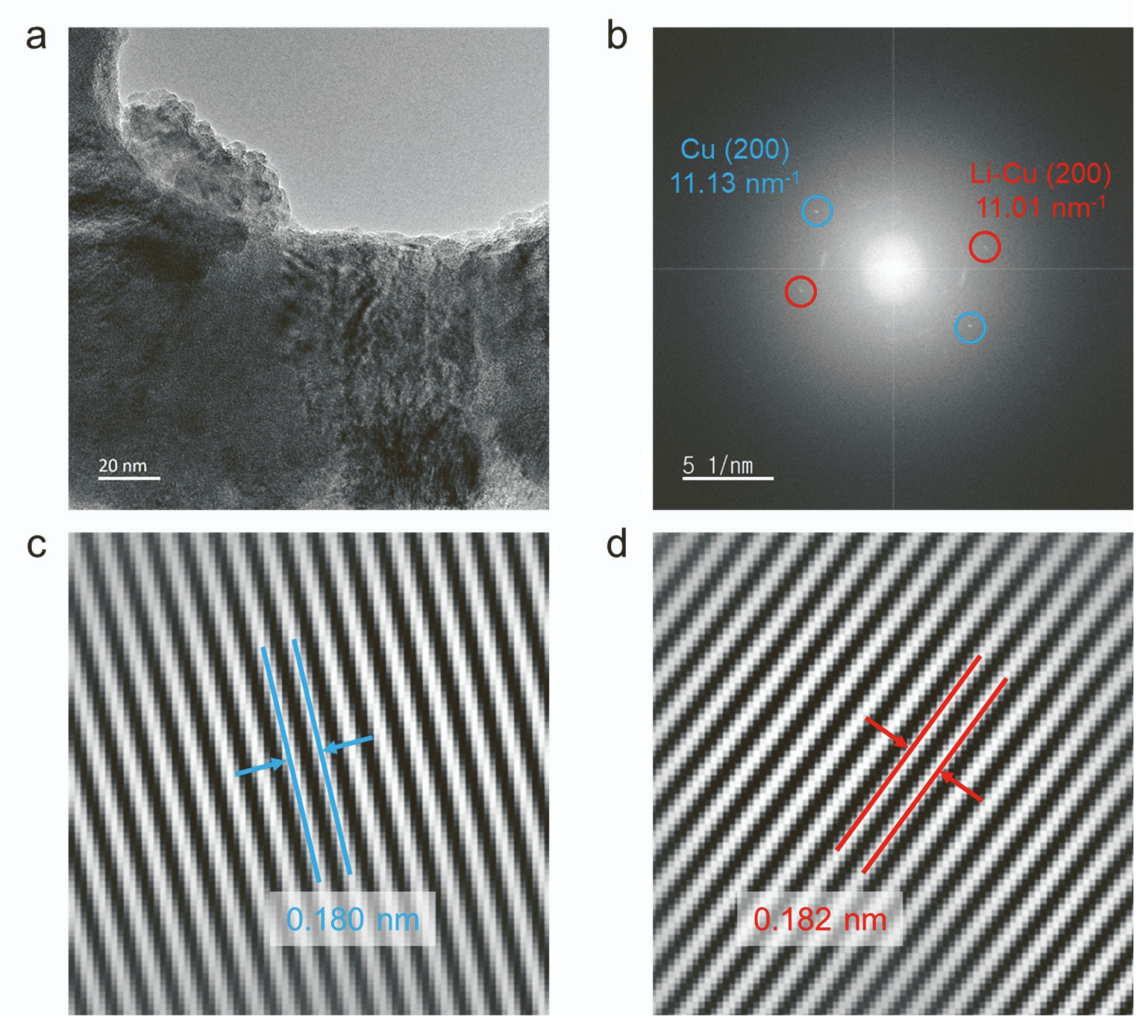

Figure S3 | TEM analysis of Li-Cu alloy. a) Bright field image and b) the corresponding FFT image. Spots highlighted in blue and red refers to Cu (200) lattice and Li-Cu (200) lattice, respectively. Inverse FFT image showing d-spacing of c) Cu (200) and d) Li-Cu (200) lattice planes.

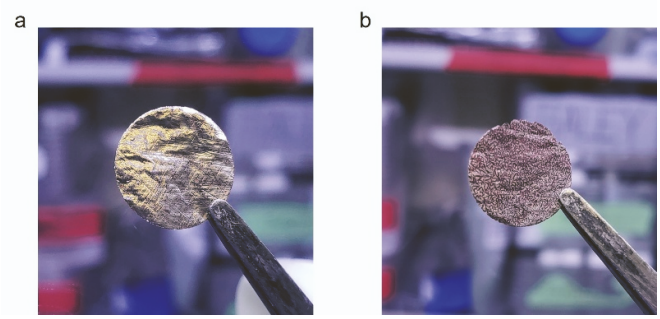

Figure S4 | Optical images of a) Li-Cu-1 and b) Li-Cu-3.

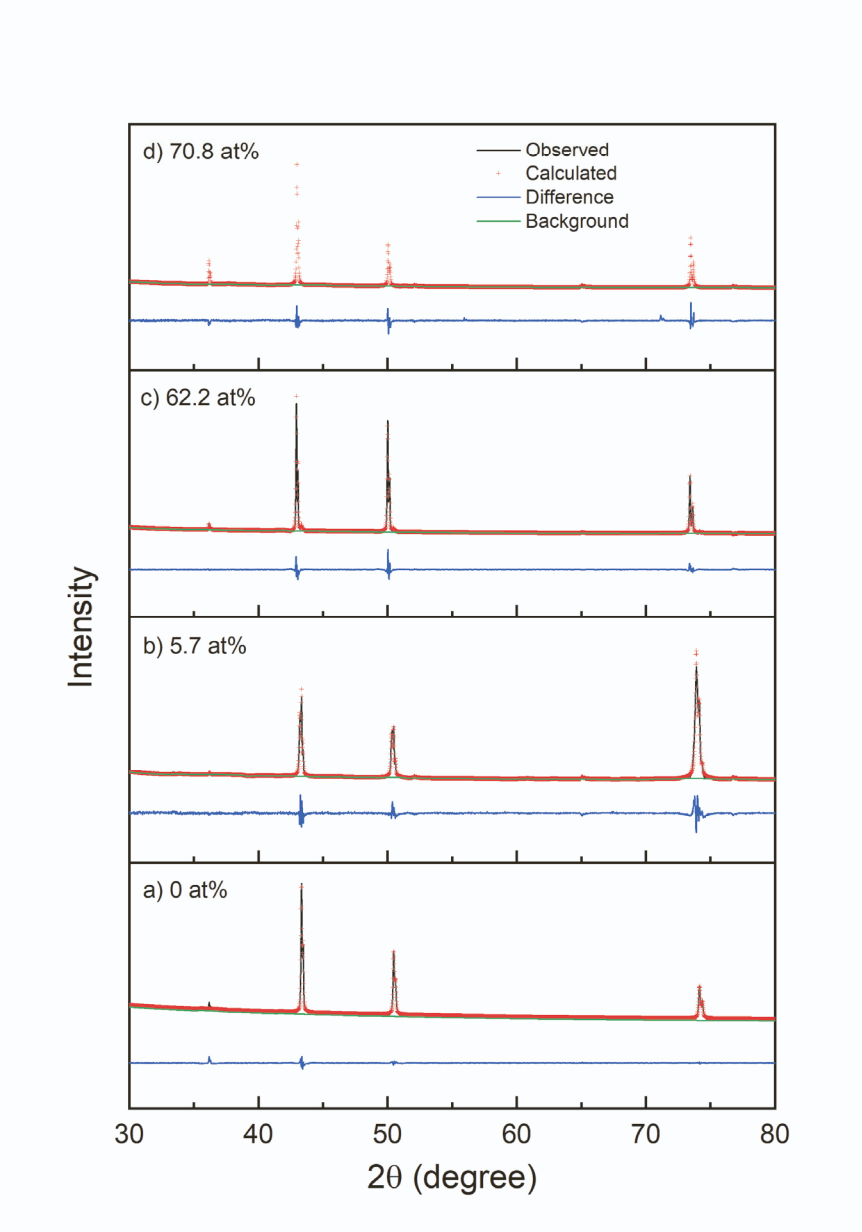

Figure S5 | Pawley fitted XRD spectra. a) Li 0 at% (before annealing), b) Li 5.7 at%, c) Li 62.2 at%, and d) Li 70.8 at%.

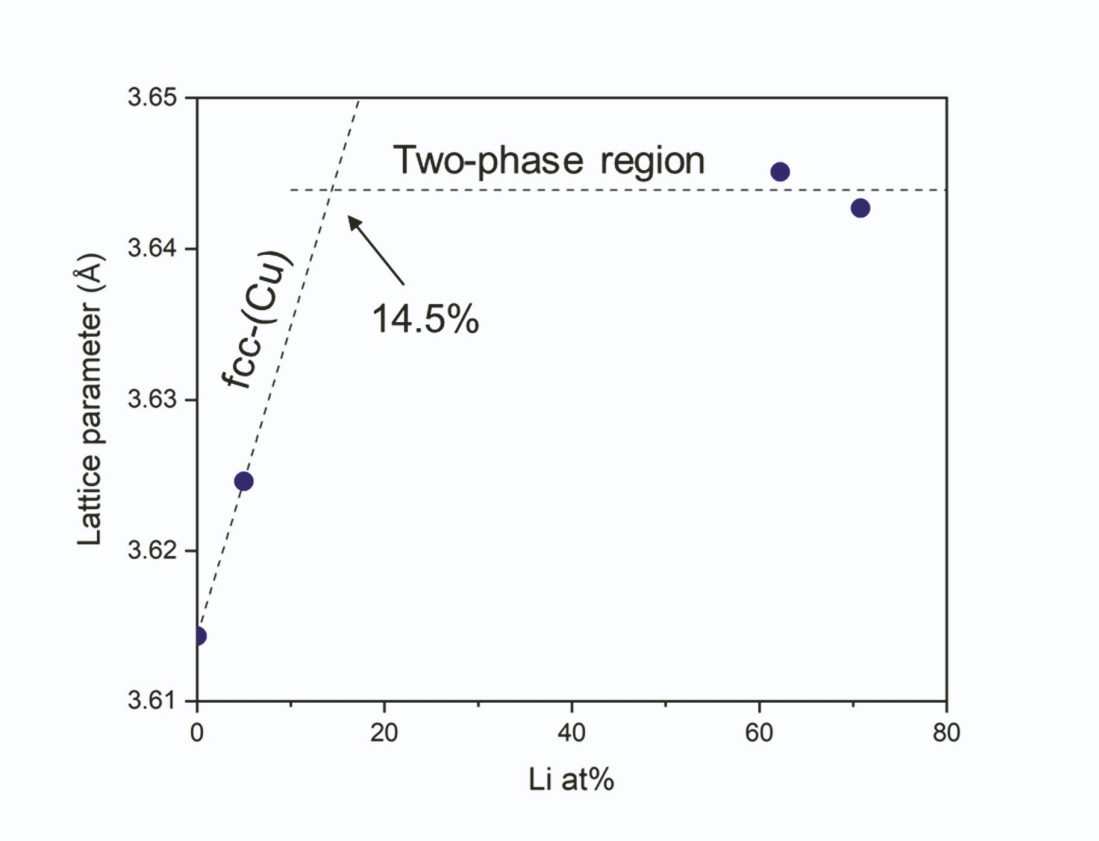

Figure S6 | Pawley fitted lattice parameters of annealed Li/Cu foils at different initial Li at%. The arrow marks the intersection of two extrapolated lines.

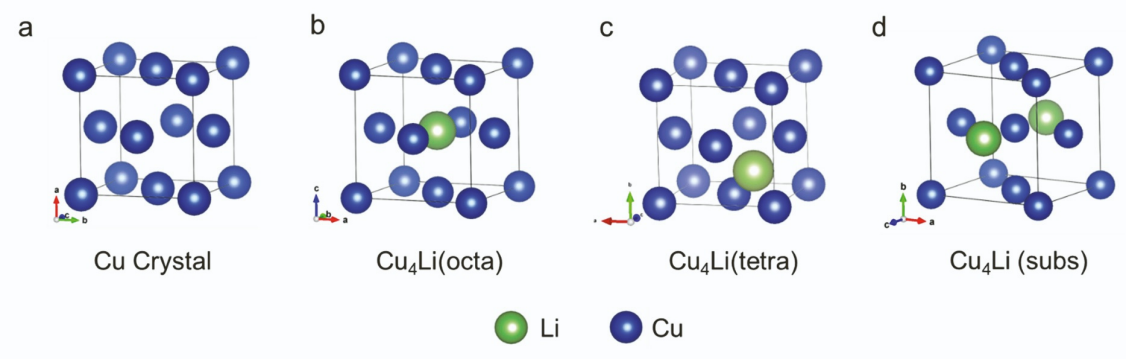

Figure S7 | Designed unit cells for DFT energy calculations. Unit cells of a) Cu, b) Cu_4Li (Li : interstitial atom at octahedral site), c) Cu_4Li (Li : interstitial atom at octahedral site) and d) Cu_4Li (Li : substitutional atom at octahedral site). (Green : Li, blue : Cu)

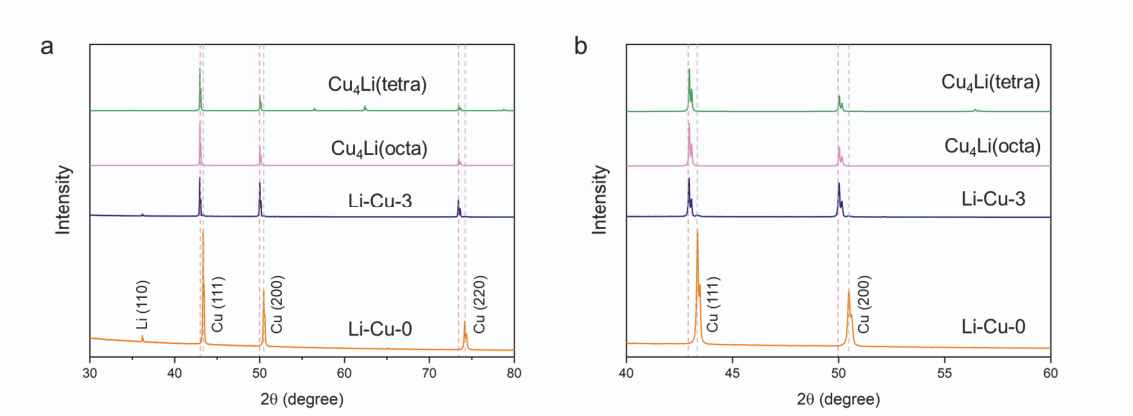

Figure S8 | Comparison of experimental XRD spectra with simulated powdered XRD spectra of Li-Cu alloy. Cu and Li-Cu peaks are marked with grey and pink dashed lines, respectively. a) XRD spectra of Li-Cu-0 (orange), Li-Cu-3 (navy), simulated Cu_4Li(octa) (pink) and Cu_4Li(tetra) (green). b) Enlarged plot showing 2θ range 40 – 60°.

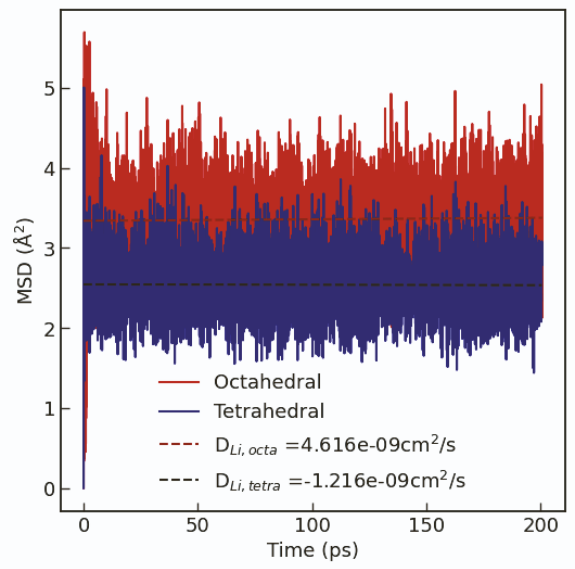

Figure S9 | AIMD simulated Li diffusion in bulk. Mean squared distances of a Li atom from an octahedral site (red) and a tetrahedral site (blue) in a Cu lattice.

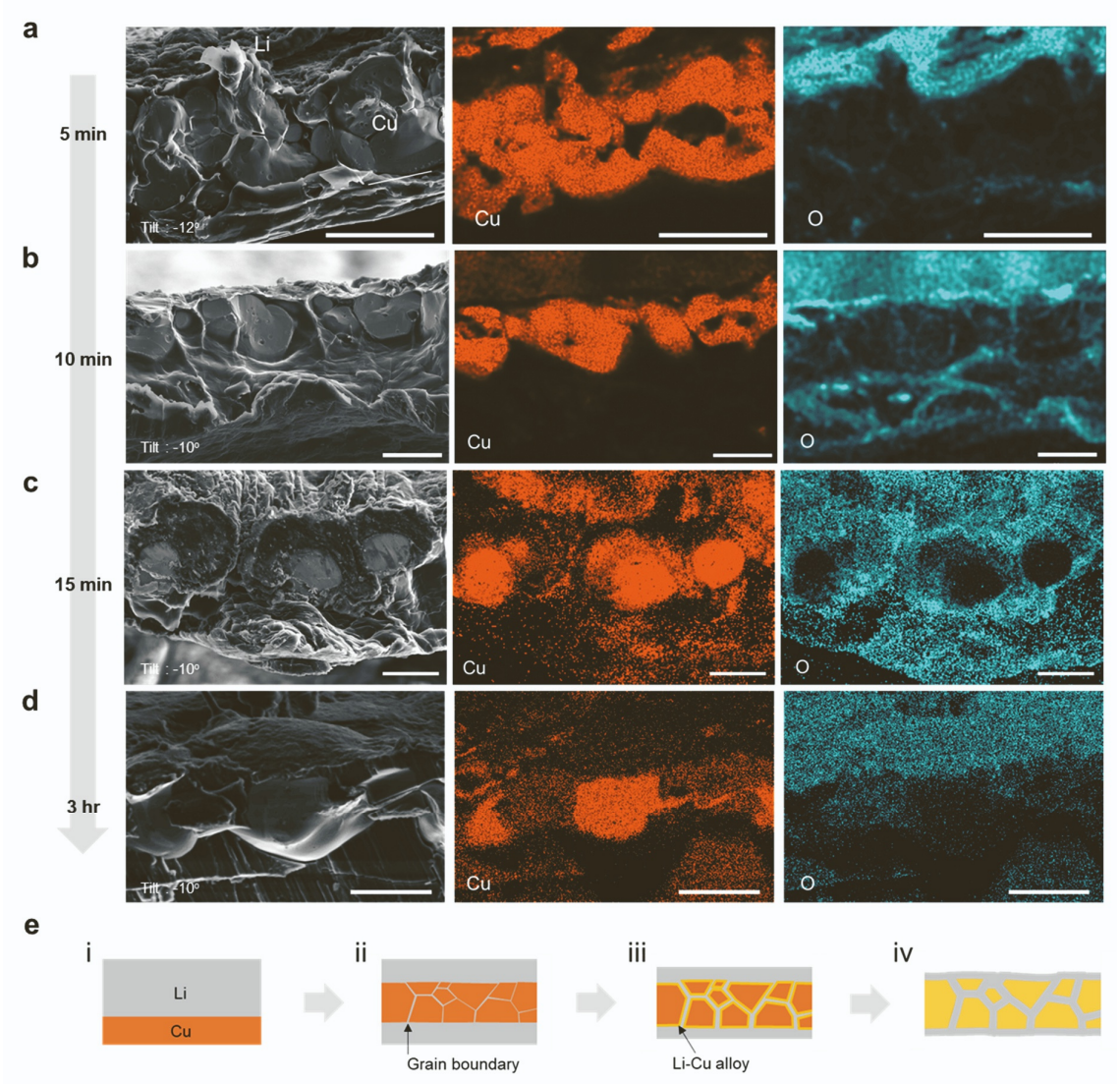

71

72 **Figure S10 | Alloying mechanism of thin Li on Cu foil.** a) Schematic figure on the formation of Li-Cu
73 alloy during annealing. i) Pristine Li thin film (grey) on Cu foil (orange) before annealing. ii) Rapid
74 diffusion of molten Li through grain boundaries at an initial stage of annealing (T > 180 °C). iii) Formation
75 of lithiophilic Li-Cu (yellow) layers on Cu grains upon further annealing. iv) Complete transformation of
76 Cu grains into Li-Cu alloy. Cross-sectional SEM image of Li on Cu foil after b) 5 min, c) 10 min, d) 15
77 min, and e) 3hr of annealing at 400 °C (left column) and corresponding EDS mapping of Cu (middle,
78 orange), and O (right, cyan). Scale bar = 20 μm.

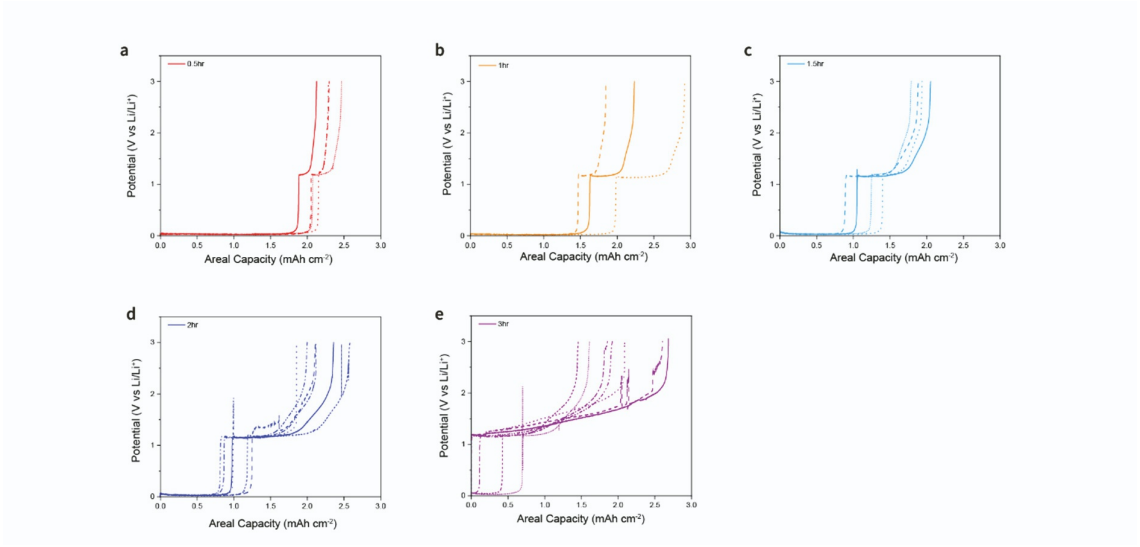

Figure S11 | Voltage profiles of Li||Li-Cu coin cells under a charging protocol to 3 V at 0.1 mA cm^{-2}. a) 0.5 hr, b) 1 hr, 3) 1.5 hr, 4) 2 hr, and e) 3 hr annealed (400 ^{o}C) Li-Cu samples were tested in 1 M LiTFSI DOL/DME (1:1) + 5 wt% $LiNO_3$ electrolyte. Multiple curves in each plot represent duplicated cells prepared for each condition.

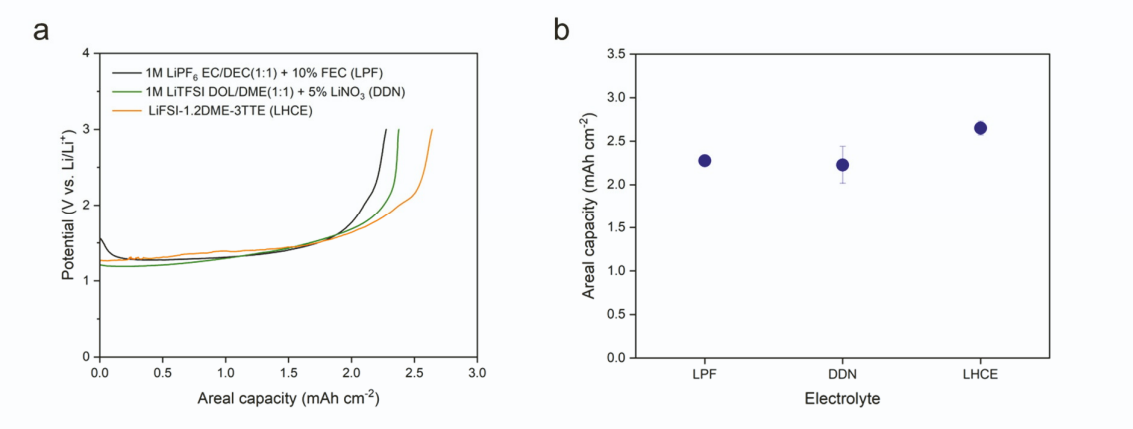

Figure S12 | Capacity of Li-Cu alloy in different electrolytes. a) Capacity stored in Li-Cu-3 was measured by extracting lithium to 3 V in 1M $LiPF_6$ EC/DEC (1:1) + 10% FEC (LPF, blue), 1M LiTFSI DOL/DME (1:1) + 5% $LiNO_3$ (DDN, green), and LiFSI-1.2DME-3TTE (localized high-concentration electrolyte, LHCE, orange). b) Comparison on areal capacities of Li-Cu (3 hr) from different electrolytes.

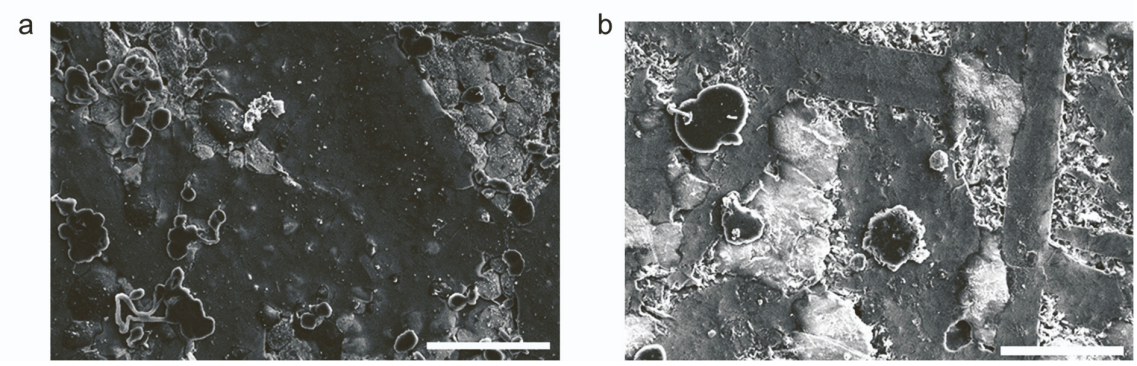

Figure S13 | Top-view SEM image of Li-Cu alloy surface after extracting stored lithium. Both a) lithium plating and subsequent b) stripping shows existence of lithium on the surface instead of re-alloying process. (Scale bar = 100 μm).

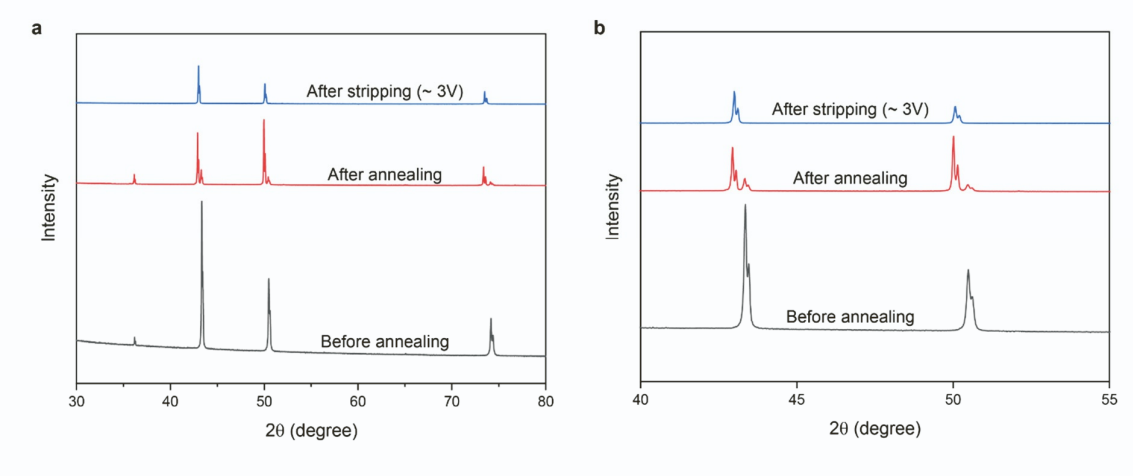

Figure S14 | Comparison of XRD results before and after Li extraction. XRD spectra of commercial Li/Cu foil before annealing (black), after annealing at 400 °C for 2 hr (red), and after annealing followed by stripping Li to 3 V (blue), shown over (a) the full 2θ range (30–80°) and (b) an enlarged range (40–55°).

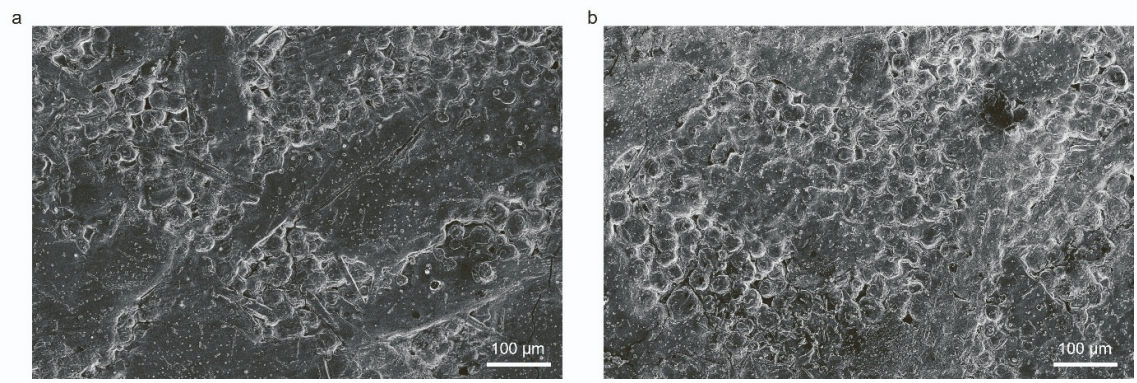

Figure S15 | SEM images of Li-Cu-3 before (a) and after stripping to 3 V (b) in 1M LiFSI DME electrolyte.

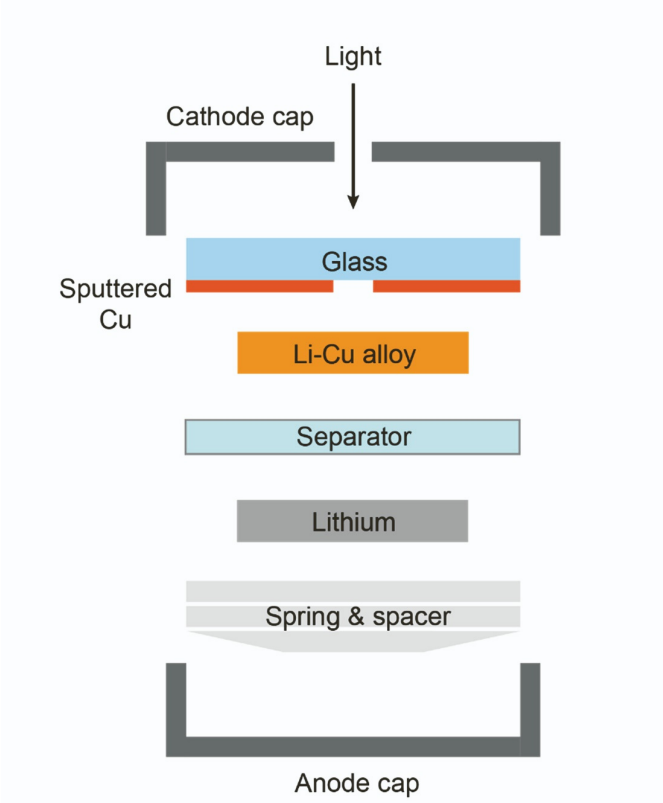

107

108 **Figure S16 | A scheme of a modified coin cell for optical microscopy.** An optical window was

109 prepared by making a hole on the cathode cap and attaching a Cu sputtered-glass on it.

110

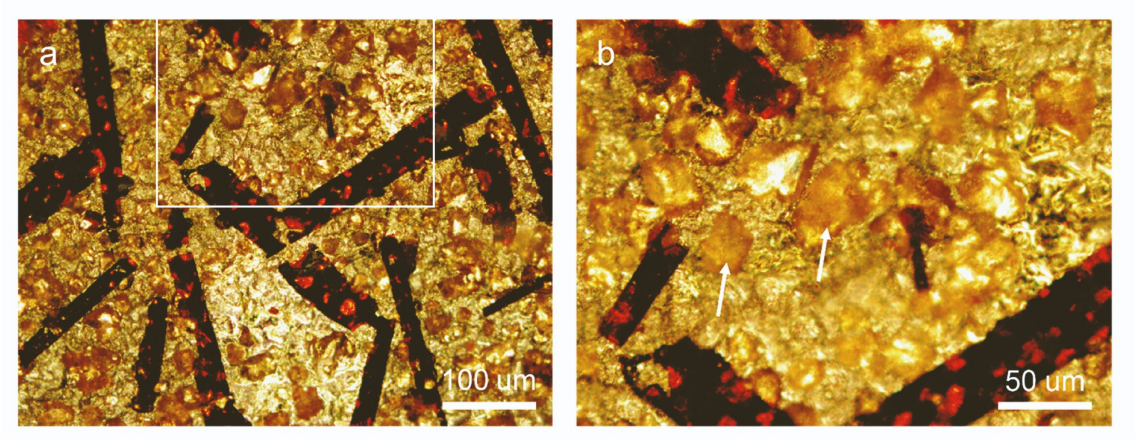

Figure S17 | Optical microscopy image of Li-Cu alloy. a) As prepared Li||Li-Cu-2 modified coin cell. b) High magnification image of the selected area in a). Arrows mark Li-Cu alloy particles covered with lithium.

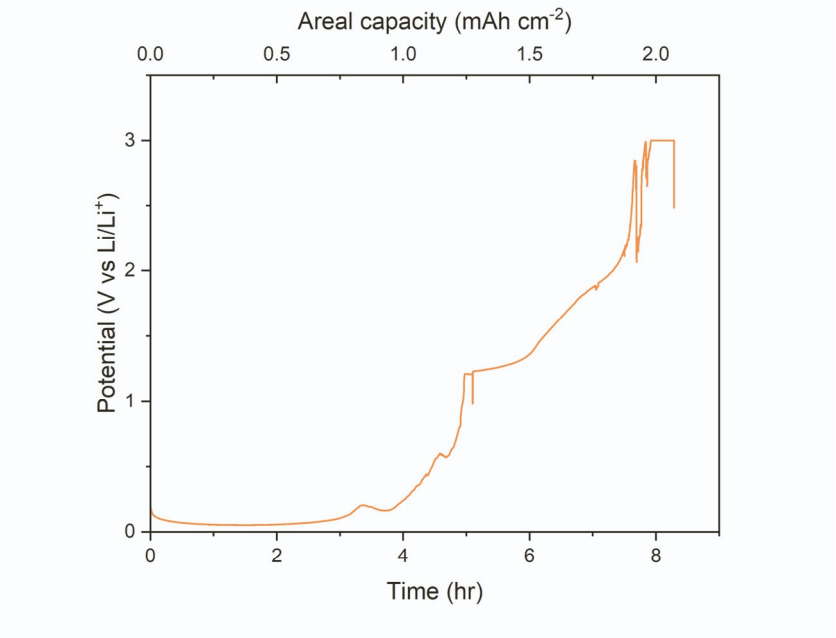

Figure S18 | Voltage profile of Li||Li-Cu-2 cell in operando optical microscopy. The cell was charged to 3 V (vs Li/Li^+) at a constant current of 0.25 mA cm^{-2}. X-axis at the bottom shows elapsed time of charging and the top axis shows total extracted areal capacity.

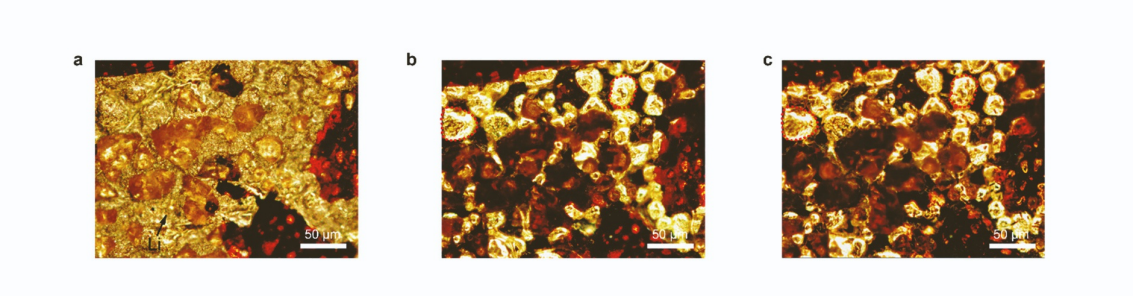

Figure S19 | Operando optical microscopy images of Li||Li-Cu-2 cell. Top-view images of Li-Cu alloy samples at a) OCV, b) 1.2 V and c) 3 V, respectively, from optical microscopy.

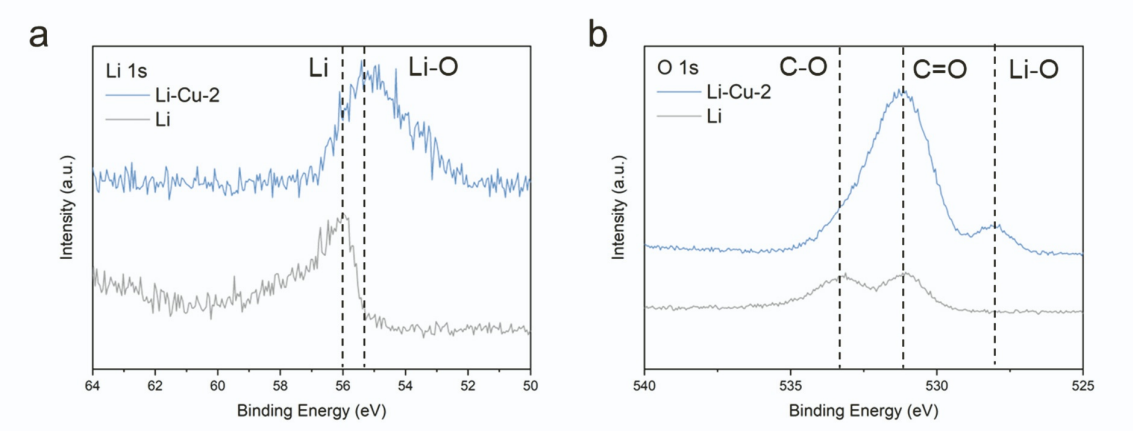

123

124 **Figure S20 | High-resolution XPS spectra of surface-scrapped Li and as-prepared Li-Cu-2.**

125 Samples were prepared without exposure to electrolyte. a) Li 1s signals. b) O 1s signals.

126

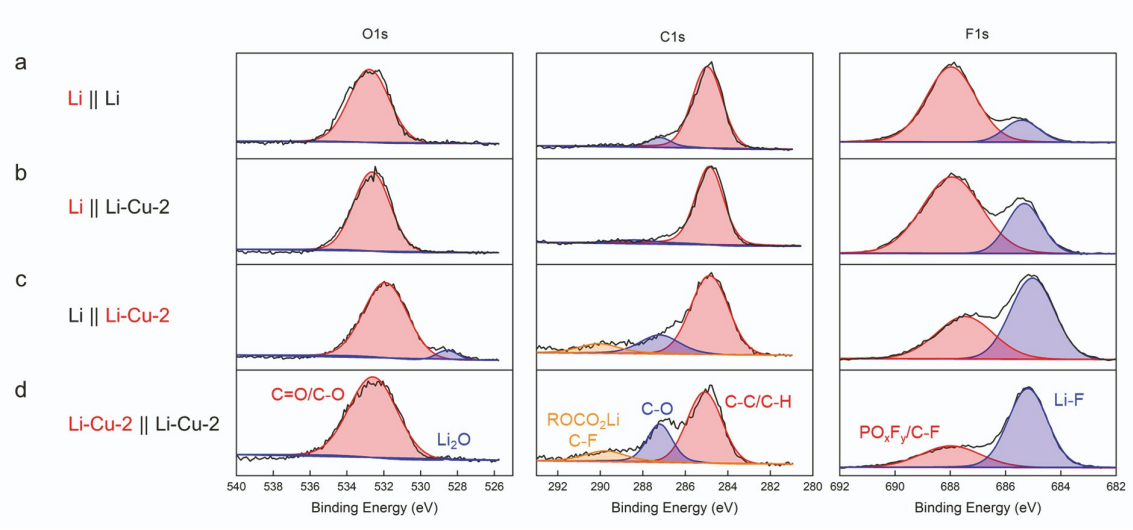

127

128 **Figure S21 | High resolution XPS spectra of Li and Li-Cu alloy surfaces after 24 hr rest in 1M**

129 **$LiPF_6$ EC/DEC (1:1) + 10% FEC electrolyte.** XPS spectra on the surface of a) Li in Li||Li cell, b) Li in

130 Li||Li-Cu cell, c) Li-Cu in Li||Li-Cu cell, and d) Li-Cu in Li-Cu||Li-Cu cell.

131

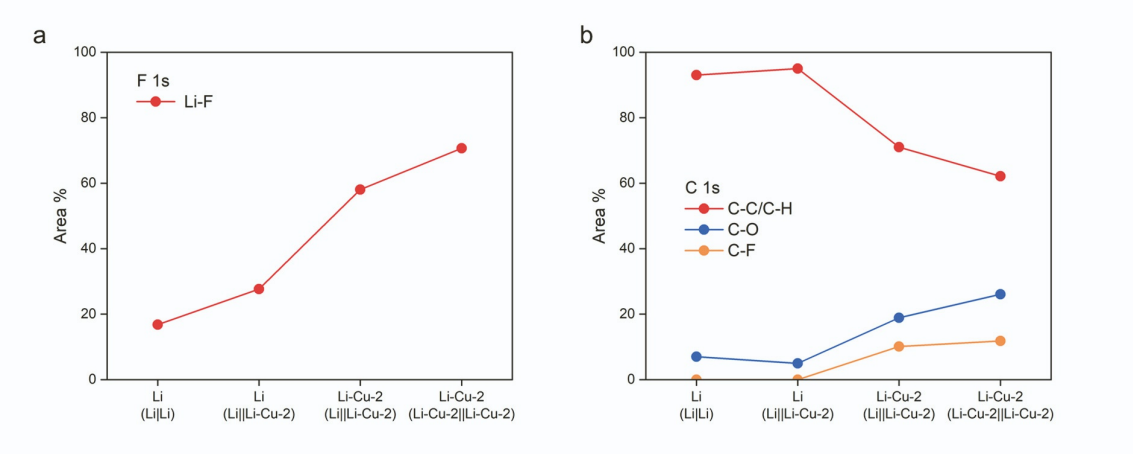

Figure S22 | Peak area % of various species from high-resolution XPS spectra. Peak area % of a) Li-F peak in F 1s spectra, and b) C-C/C-H (red), C-O (blue), and C-F (orange) peaks in O 1s spectra.

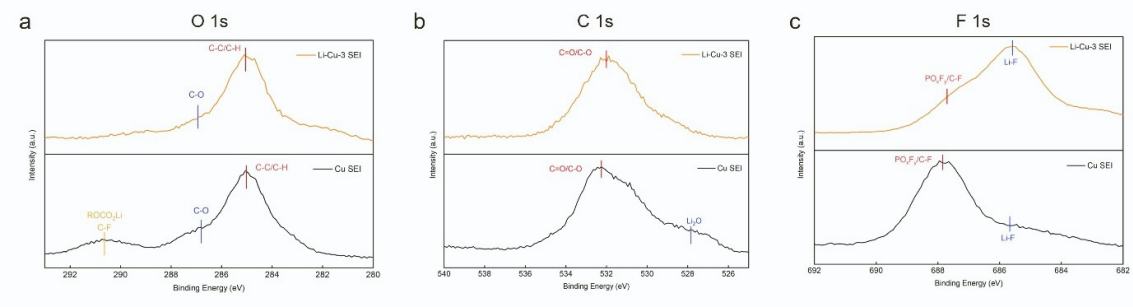

136

137 **Figure S23 | High-resolution XPS spectra of SEI formed by constant-current voltage protocol**

138 **on Cu (black) and Li-Cu-3 (orange).** O 1s (a), C 1s (b), and F 1s (c) spectra are shown and labelled

139 with corresponding functional groups.

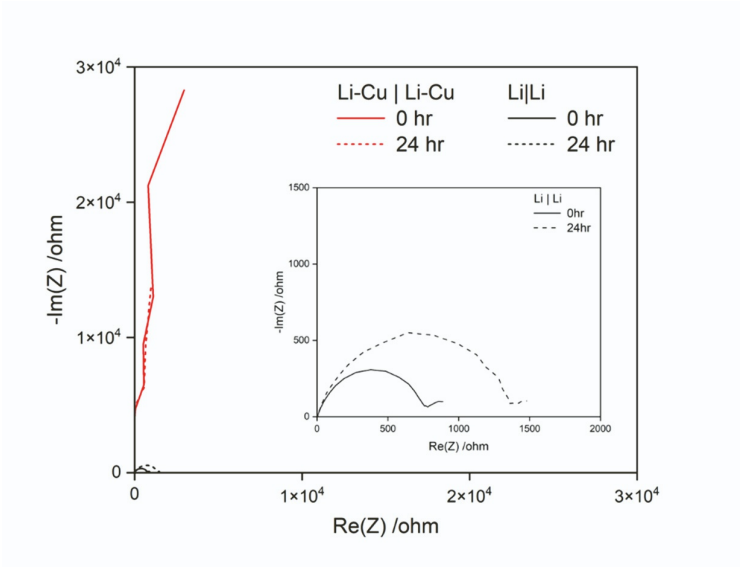

Figure S24 | Electrochemical impedance analysis (EIS) of Li-Cu-2||Li-Cu-2 (red line) and Li||Li symmetric cells with LPF electrolyte. EIS measurements were made at 0 hr (solid line) and after 24 hr (dashed line) the fabrication of cells. Inset shows larger view of Li||Li cell data.

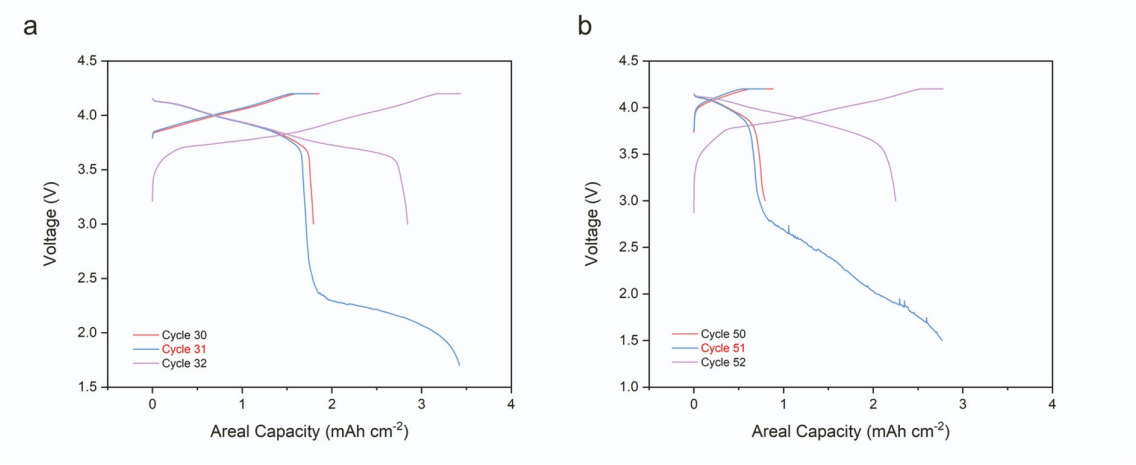

Figure S25 | Voltage profiles of Li-Cu-3||NMC811 full cells in LPF electrolyte before and after extraction steps. Charge-discharge curves at a) cycles 30-32 (extraction at 31st cycle, highlighted in red), and b) cycles 50-52 (extraction at 51st cycle, highlighted in red).

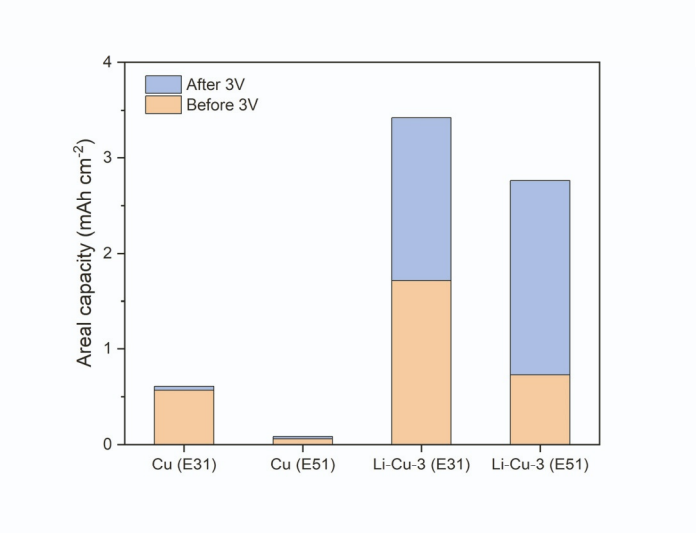

Figure S26 | Discharge capacity of anode-free NMC811 full cells with LPF electrolyte during the extraction cycle. Capacity before and after reaching 3V is denoted as 'Before 3V' (orange) and 'After 3V' (blue), respectively. E31 and E51 refer to the extraction cycles located at the 31st cycle and the 51st cycle, respectively.

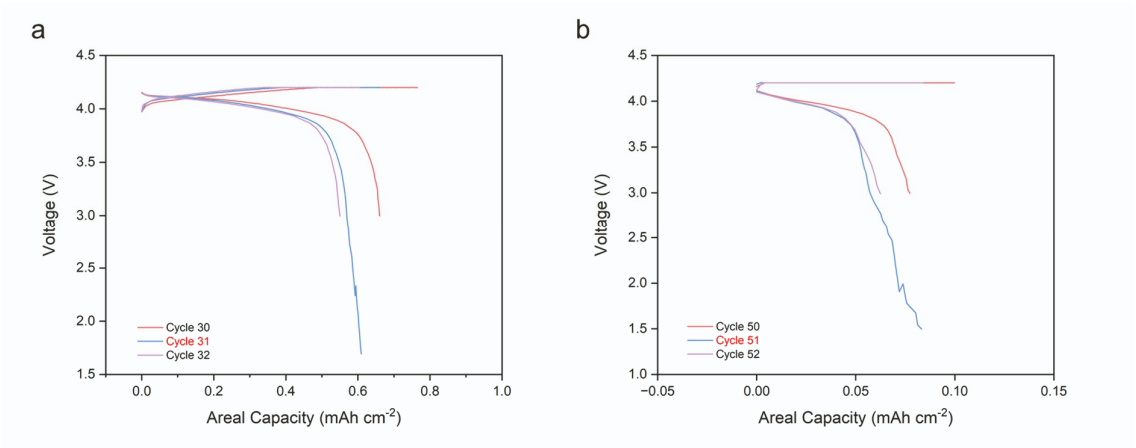

Figure S27 | Voltage profiles of Cu||NMC811 full cells in LPF electrolyte before and after extraction steps. Charge-discharge curves at a) cycles 30-32 (extraction at 31st cycle), and b) cycles 50-52 (extraction at 51st cycle).

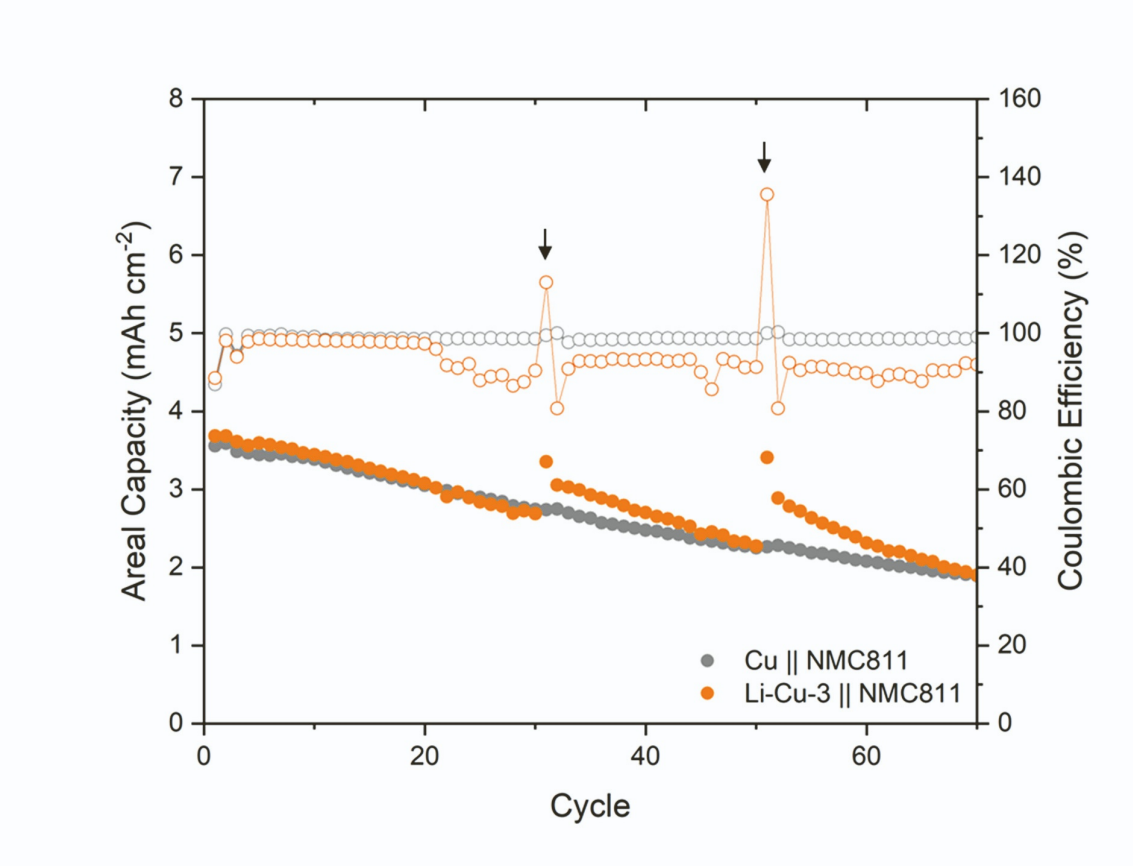

Figure S28 | Representative cycling data of anode-free full cells (Cu||NMC811 (grey) & Li-Cu-3||NMC811 (orange)) with LHCE electrolyte (LiFSI - 1.2 DME – 3 TTE electrolyte). For both types, multiple extraction steps were conducted at 31st cycle (to 1.7 V) and 51st cycle (to 1.5 V) (marked with arrows). Cells were cycles with a CC-CV protocol (0.2 C charging – constant voltage at 4.2 V (down to 0.05 C) – 0.3 C discharging).

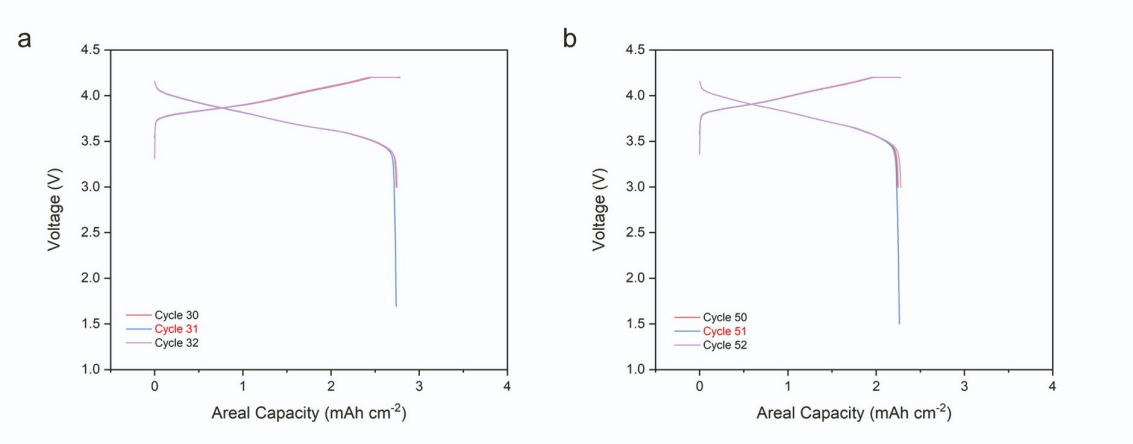

Figure S29 | Voltage profiles of Cu||NMC811 full cells (LiFSI - 1.2 DME – 3 TTE electrolyte) before and after extraction steps. Charge-discharge curves at a) cycles 30-32 (extraction at 31st cycle), and b) cycles 50-52 (extraction at 51st cycle).

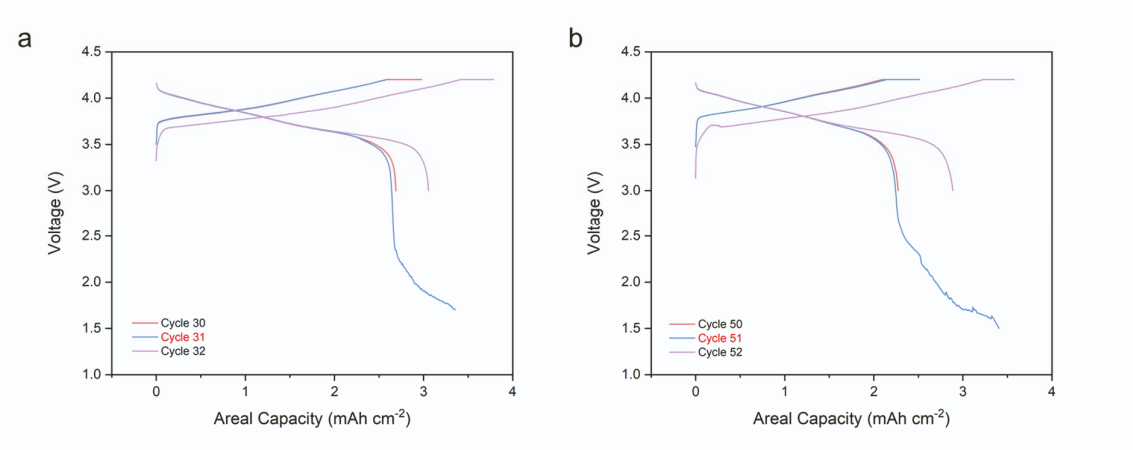

Figure S30 | Voltage profiles of Li-Cu-3||NMC811 full cells (LiFSI - 1.2 DME – 3 TTE electrolyte) before and after extraction steps. Charge-discharge curves at a) cycles 30-32 (extraction at the 31st cycle), and b) cycles 50-52 (extraction at the 51st cycle).

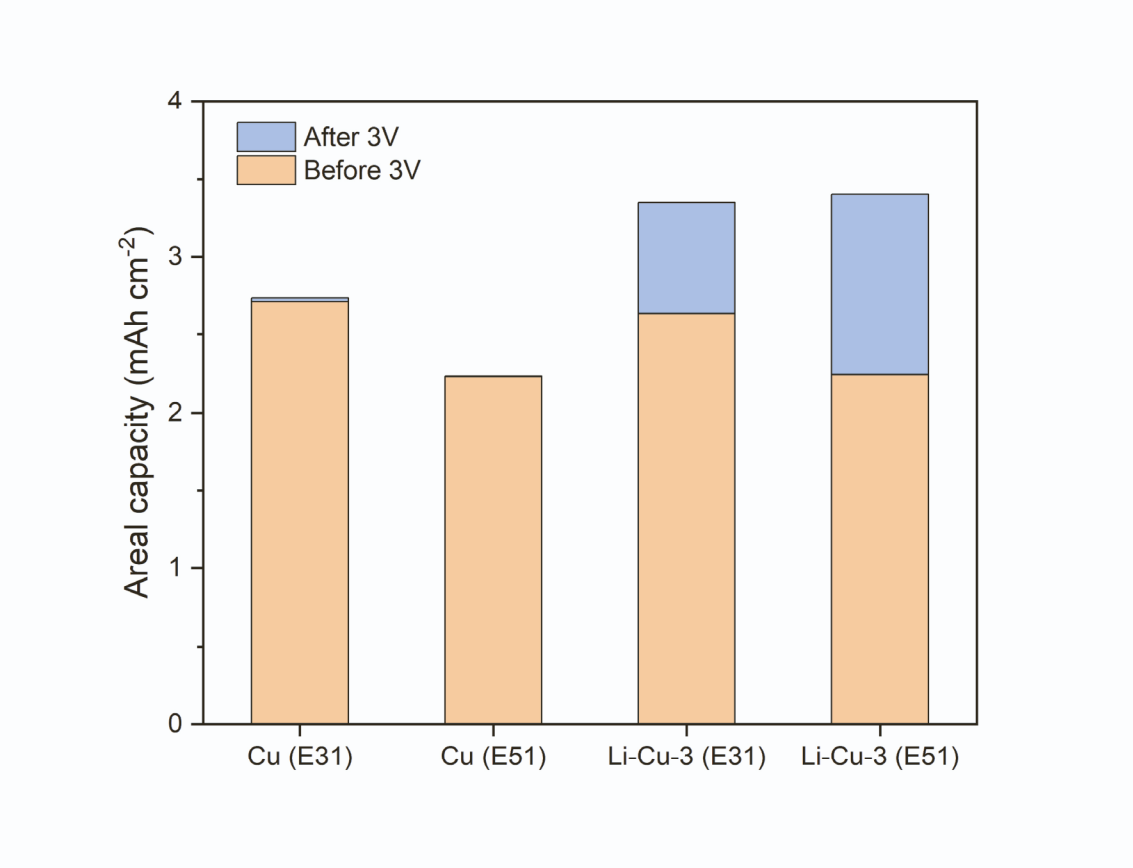

Figure S31 | Discharge capacity of anode-free NMC811 full cells with LHCE electrolyte above and below cell voltage of 3V during the extraction cycle. Capacity before and after reaching 3V is denoted as 'Before 3V' (orange) and 'After 3V' (blue), respectively. E31 and E51 refer to the extraction cycles located at the 31st cycle and the 51st cycle, respectively.

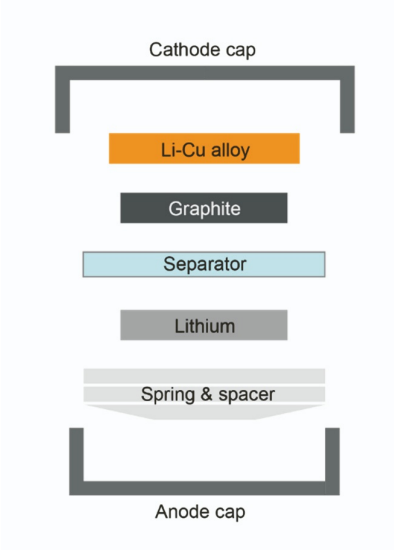

Figure S32 | A scheme showing the structure of Li||Gr + Li-Cu coin cell. Freestanding Gr electrode was placed on the cathode side with Li-Cu alloy as a CC.

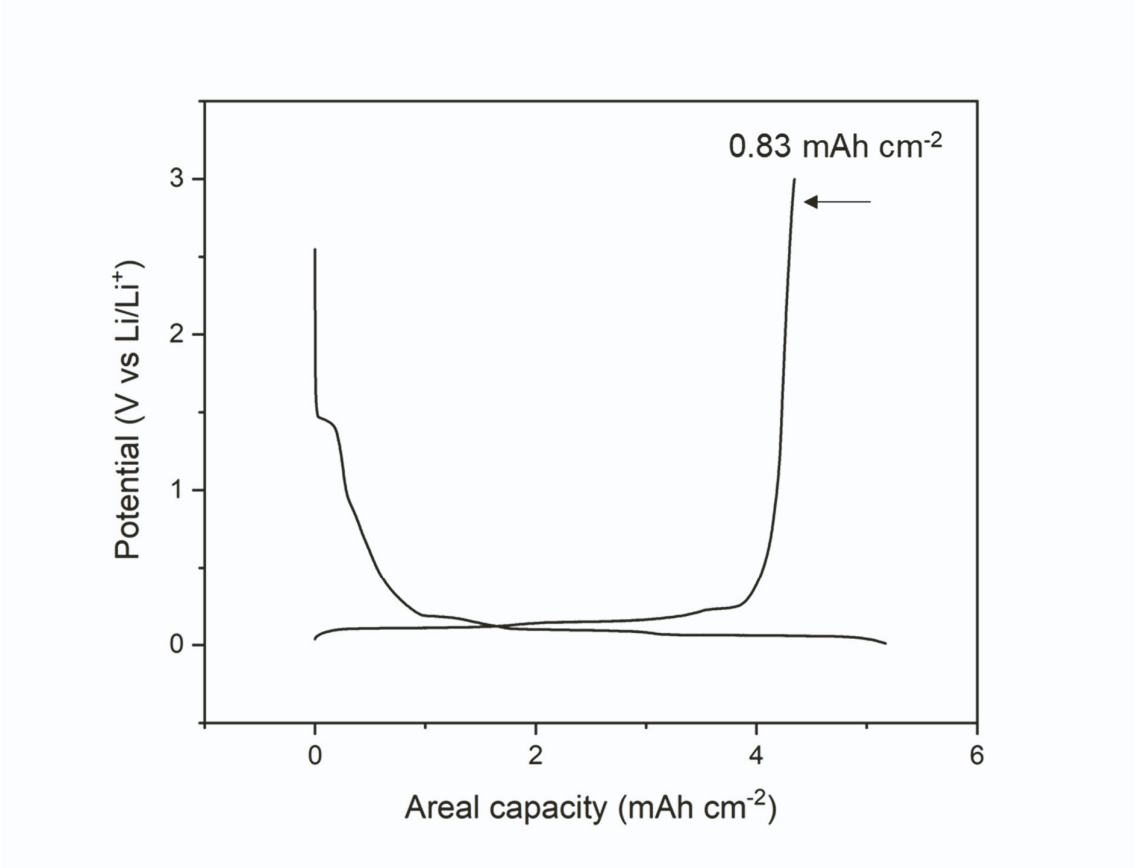

Figure S33 | Voltage profiles of Li||Gr half cycled at 0.05 C in LPF electrolyte against areal capacity in the first cycle. The capacity loss in the initial cycle was ~ 0.83 mAh cm^{-2}.

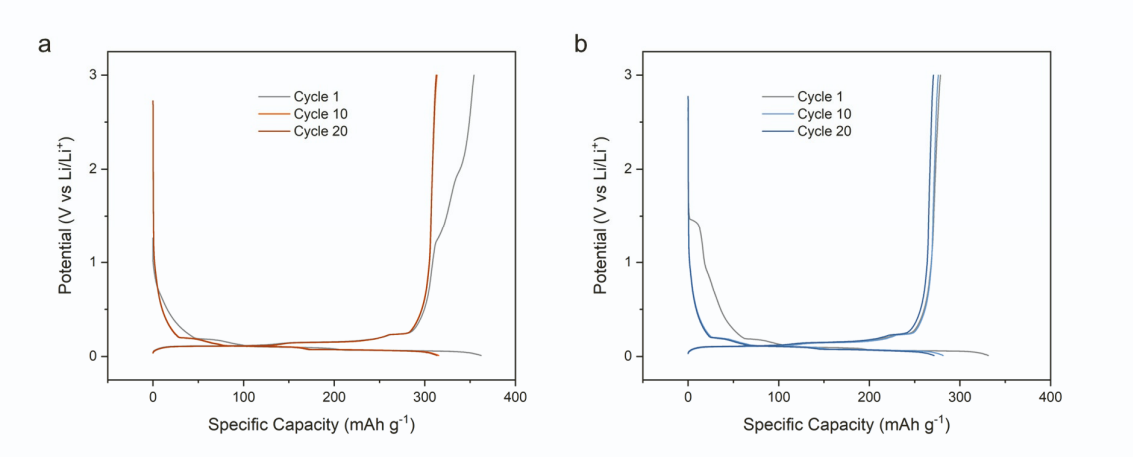

194

195 **Figure S34 | Charge-discharge curves of Gr-based half cells cycled at 0.05 C in 1M $LiPF_6$ EC:DEC**
196 **(1:1) + 10% FEC electrolyte.** a) Voltage profiles of Li||Gr+Li-Cu-2 half cell at cycle 1 (grey), 10 (orange),
197 and 20 (brown). b) Voltage profiles of Li||Gr half cell at cycle 1 (grey), 10 (light blue), and 20 (blue).

198

199

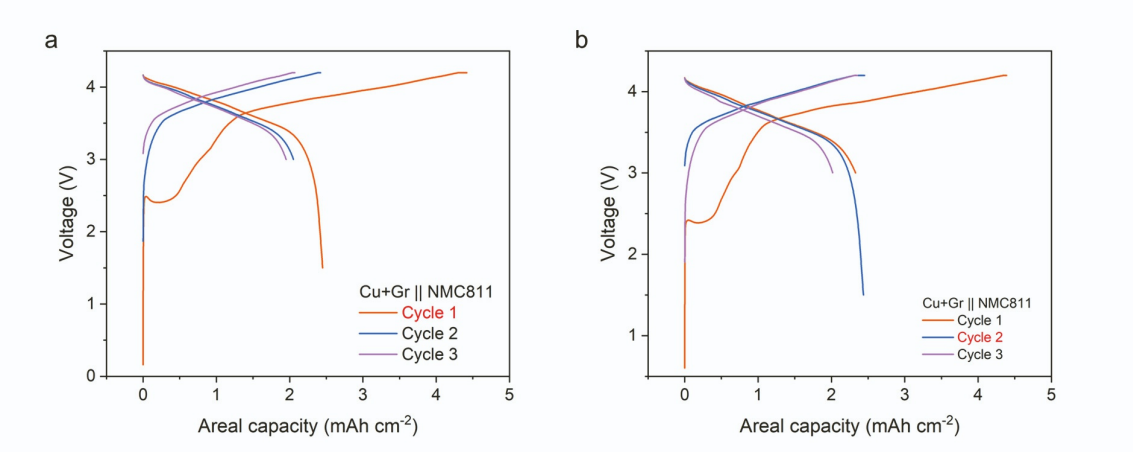

200

201 **Figure S35 | Voltage profiles of Cu+Gr||NMC811 full cells in LPF electrolyte before and after**
202 **extraction steps.** Charge-discharge curves of first 3 cycles from a) E1 and b) E2 protocols.

203

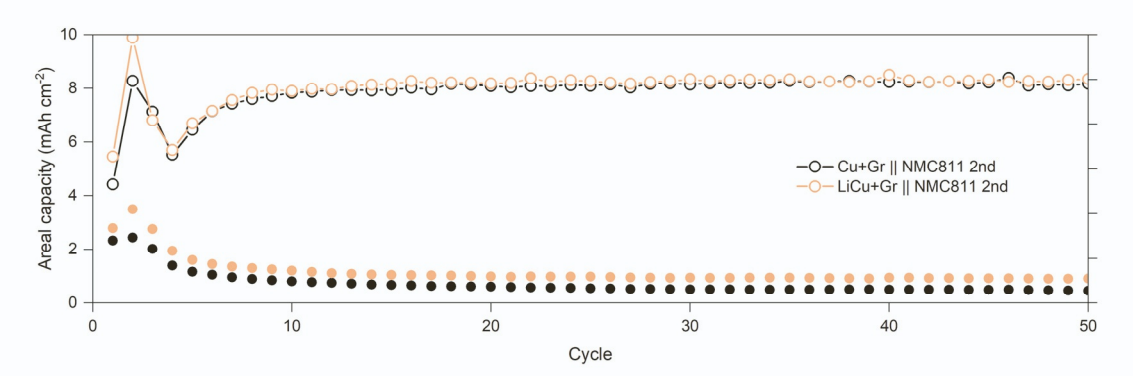

Figure S36 | Representative cycling profiles of Cu+Gr||NMC811 and Li-Cu-3+Gr||NMC811 full cells with the extraction steps on the 2nd cycles (E2). The CE (open circle) and the discharge areal capacity (filled circle) are shown. The cycling was performed at 0.1C (3 cycles) and 0.5C afterwards.

Li at%	Cu (F m -3 m)	Li-Cu	Li (I m -3 m)
0	3.6143	-	3.5093
5.7	3.6134	3.6246	3.5094
62.2	3.6135	3.6451	3.5094
70.8	3.6135	3.6427	3.5096

209

210 **Table S1**. **| Pawley fitted lattice parameters of Cu, Li-Cu alloy and Li**. α=β=γ=90° and a=b=c values

211 are given in the table (unit : Å for lattice parameters).